Inorganic Chemistry
Article
Cite This: Inorg. Chem. 2019, 58, 4152−4163
pubs.acs.org/IC

^{13}C NMR Shifts as an Indicator of U−C Bond Covalency in Uranium(VI) Acetylide Complexes: An Experimental and Computational Study

Kimberly C. Mullane,[†] Peter Hrobárik,*[,‡,§] Thibault Cheisson,[†] Brian C. Manor,[†] Patrick J. Carroll,[†] and Eric J. Schelter*[,†]

[†]P. Roy and Diana T. Vagelos Laboratories, Department of Chemistry, University of Pennsylvania, 231 South 34th Street, Philadelphia, Pennsylvania 19104, United States

[‡]Department of Inorganic Chemistry, Faculty of Natural Sciences, Comenius University, SK-84215 Bratislava, Slovakia

[§]Institut für Chemie, Technische Universität Berlin, Straße des 17. Juni 135, D-10623 Berlin, Germany

Supporting Information

ABSTRACT: A series of uranium(VI)−acetylide complexes of the general formula $U^{VI}(O)(C{\equiv}C{-}C_6H_4{-}R)[N(SiMe_3)_2]_3$, with variation of the *para* substituent (R = NMe_2, OMe, Me, Ph, H, Cl) on the aryl(acetylide) ring, was prepared. These compounds were analyzed by ^{13}C NMR spectroscopy, which showed that the acetylide carbon bound to the uranium(VI) center, U−C≡C−Ar, was shifted strongly downfield, with $\delta(^{13}C)$ values ranging from 392.1 to 409.7 ppm for Cl and NMe_2 substituted complexes, respectively. These extreme high-frequency ^{13}C resonances are attributed to large negative paramagnetic (σ^{para}) and relativistic spin−orbit (σ^{SO}) shielding contributions, associated with extensive U(5f) and C(2s) orbital contributions to the U−C bonding in title complexes. The trend in the ^{13}C chemical shift of the terminal acetylide carbon is opposite that observed in the series of parent (aryl)acetylenes, due to shielding effects of the *para* substituent. The ^{13}C chemical shifts of the acetylide carbon instead correlate with DFT computed U−C bond lengths and corresponding QTAIM delocalization indices or Wiberg bond orders. SQUID magnetic susceptibility measurements were indicative of the Van Vleck temperature independent paramagnetism (TIP) of the uranium(VI) complexes, suggesting a magnetic field-induced mixing of the singlet ground-state (f^0) of the U(VI) ion with low-lying (thermally inaccessible) paramagnetic excited states (involved also in the perturbation-theoretical treatment of the unusually large paramagnetic and SO contributions to the ^{13}C shifts). Thus, together with reported data, we demonstrate that the sensitive ^{13}C NMR shifts serve as a direct, simple, and accessible measure of uranium(VI)−carbon bond covalency.

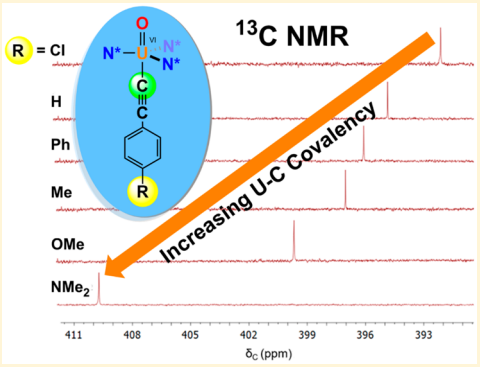

Downloaded by UNIV OF PENNSYLVANIA at 07:09:47:621 on June 04, 2019
from https://pubs.acs.org/doi/10.1021/acs.inorgchem.8b03175.

INTRODUCTION

Interest in organometallic uranium complexes developed in the 1950s for applications in isotope separations processes. Actinide organometallic complexes were expected to be volatile, in analogy with transition metal organometallic complexes.[1,2] Since that time, a number of uranium(IV) alkyl complexes have been synthesized, supported by substituted cyclopentadienyl,[3−6] amide,[7−10] alkoxide,[11] phosphine,[12,13] and homoleptic ligand frameworks.[14−17] However, uranium alkyl complexes in the oxidation states III,[18,19] V,[20] and VI[10,20,21] remain relatively scarce. Among the known organometallic uranium complexes are a number of uranium(IV) acetylide complexes.[22−32] However, as in the chemistry of uranium alkyls, there are few examples of uranium acetylides in the other available oxidation states of uranium.[10,25,33]

Work from our group recently reported the first example of a uranium(VI) acetylide complex, $U^{VI}(O)(C{\equiv}C{-}Ph)[N(SiMe_3)_2]_3$ (**1-H**), stabilized through the inverse *trans* influence by the *trans* position of the (phenyl)acetylide ligand with respect to an oxo ligand.[10] The axial U−C bond in this compound was short (2.337(14) Å) when compared with equatorial U−C bonds, as in the uranyl−alkyl complex reported by Hayton and co-workers, $[Li(DME)_{1.5}]_2[U^{VI}O_2(CH_2SiMe_3)_4]$ (2.489(6) Å; Figure 1).[34] For equatorial U−C interactions with more dative bonding, as in $U^{VI}O_2Cl[HC(PPh_2NMes)_2](THF)$ (Mes = C_6H_2-2,4,6-Me_3), reported by Liddle and co-workers, longer bonds of 2.7935(17) Å were observed.[35] When comparing within this series of compounds, the ^{13}C NMR spectra of $U^{VI}O_2Cl[HC(PPh_2NMes)_2](THF)$ and **1-H**, recorded in benzene-d_6 at room temperature, revealed that the chemical shift of the U−C carbon atom ranged from 7 to 395 ppm, respectively. These chemical shifts indicated that long U−C bonds (2.7935(17) Å) had ^{13}C resonances similar to those of free, diamagnetic ligands, while carbon atoms with short U−C bonds (2.337(14)

Received: November 12, 2018
Published: March 8, 2019

© 2019 American Chemical Society

DOI: 10.1021/acs.inorgchem.8b03175
Inorg. Chem. 2019, 58, 4152−4163

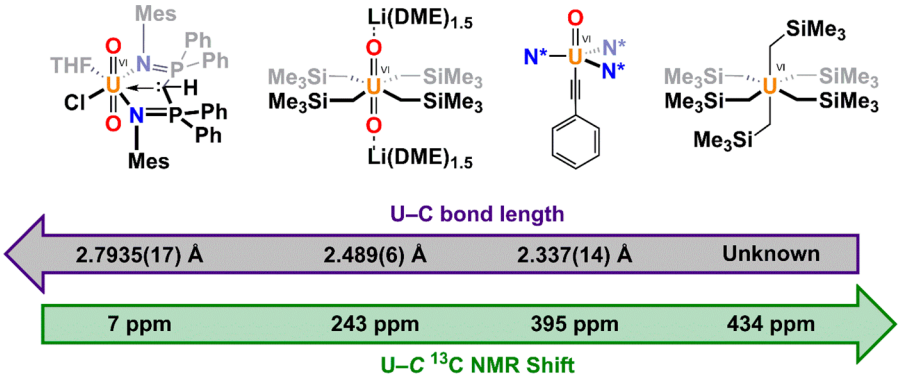

Figure 1. Selected previously reported uranium(VI) organometallic complexes, the experimental U−C bond lengths (in Å), and ^{13}C chemical shifts (in ppm with respect to TMS) of the U−C carbon. The ^{13}C NMR spectra of $U^{VI}O_2Cl[HC(PPh_2NMes)_2](THF)$ and $U^{VI}(O)(C{\equiv}C{-}Ph)[N(SiMe_3)_2]_3$ (**1-H**) were collected at room temperature in benzene-d_6. The ^{13}C NMR spectra of $[Li(DME)_{1.5}]_2[U^{VI}O_2(CH_2SiMe_3)_4]$ and $U^{VI}(CH_2SiMe_3)_6$ were recorded at −1.6 and −45.5 °C, respectively, in THF-d_8.[10,20,34,35]

Å) were shifted strongly downfield, usually beyond the typical range of diamagnetic substances (Figure 1).[36,37] The homoleptic alkyl compound, $U^{VI}(CH_2SiMe_3)_6$, reported by Hayton and co-workers, has shown the most downfield shifted resonance, at 434 ppm, recorded at −46 °C in THF-d_8, with a short calculated U−C bond length of 2.335 Å, although no crystal structure was obtained (Figure 1).[20,34]

Previously, information about bonding and electronic structure was obtained by Hrobárik and co-workers from correlating experimental and computed ^{77}Se and ^{125}Te chemical shifts of high valent actinide complexes bearing actinide-chalcogen multiple bonds.[38] Also, ^{13}C NMR spectroscopy has been used to examine the covalency of U−C bonds in two isolated uranium(VI) complexes, $[Li(DME)_{1.5}]_2[U^{VI}O_2(CH_2SiMe_3)_4]$ and $U^{VI}(CH_2SiMe_3)_6$.[34] NLMO (natural localized molecular orbital) hybridization analysis revealed that $U^{VI}(CH_2SiMe_3)_6$ had increased the uranium contribution to the U−C bond compared with $[Li(DME)_{1.5}]_2[U^{VI}O_2(CH_2SiMe_3)_4]$, with metal-based contributions of 28.9 and 21.9%, respectively. This covalency was reflected in the chemical shift of the uranium-bound carbon, which was shifted downfield to 434 ppm for $U^{VI}(CH_2SiMe_3)_6$, compared with 243 ppm for $[Li(DME)_{1.5}]_2[U^{VI}O_2(CH_2SiMe_3)_4]$ (Figure 1).[20,34]

These data indicated that increased U(VI)−C covalency within structurally related series could be evaluated in the extent of the downfield chemical shift in ^{13}C NMR spectroscopy. However, only a few examples of uranium(VI) organometallic complexes have been isolated, which prevents this observation from being further substantiated. Herein, we present the synthesis and characterization of a series of uranium(VI) (aryl)acetylide complexes with varying substitution in the *para* position, $U^{VI}(O)(C{\equiv}C{-}C_6H_4{-}R)[N(SiMe_3)_2]_3$ (R = NMe_2, OMe, Me, Ph, H, Cl; **1-R**). These complexes exhibited extreme downfield chemical shifts of the uranium-bound acetylide carbon, U−C≡C−Ar, ranging from 409.7 to 392.1 ppm. Computed U−C bond lengths and Quantum Theory of Atoms in Molecules (QTAIM) delocalization indices and Wiberg bond orders were used to determine the extent of U−C covalency. QTAIM computational methods have recently been used to examine actinide−ligand (An−L) bond covalency in a number of reported compounds.[38−46] These computational metrics are shown here to correlate well with the downfield ^{13}C chemicals shifts we observed for the uranium-bound acetylide carbon.

RESULTS AND DISCUSSION

Synthesis and Characterization of Uranium(VI) (Phenyl)Acetylide Complexes. Previously, compound **1-H** had been synthesized and reported by our group (Scheme 1).[10] The synthesis of **1-H** was accomplished by reaction of

Scheme 1. Synthesis of Uranium(VI) Acetylide Complexes 1-R (R = NMe_2, OMe, Me, Ph, H, Cl)

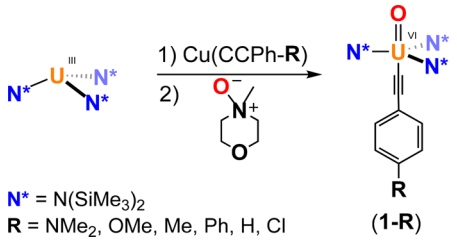

$U^{III}[N(SiMe_3)_2]_3$ with CuCCPh in a solution of diethyl ether. This reaction generated the uranium(IV) (phenyl)acetylide complex, $U^{IV}(C{\equiv}CPh)[N(SiMe_3)_2]_3$. This compound was then reacted with *N*-methylmorpholine *N*-oxide, an oxygen-atom transfer reagent, to yield **1-H** as a crystalline solid (59% yield). In order to generate a library of uranium(VI) (aryl)acetylide complexes with varying substituents in the *para* position, we employed a similar synthetic strategy and generated **1-R** (R = NMe_2, OMe, Me, Ph, Cl) complexes in low to moderate crystalline yields of 3−28% (Scheme 1). ^1H NMR spectra of crude mixtures showed that **1-R** were the major products and that the low yields were mainly due to isolation; the products were difficult to crystallize due to their high solubilities in organic solvents.

Compounds **1-R** (R = NMe_2, OMe, Me, Ph, H, Cl) were characterized by X-ray diffraction as well as by ^1H and ^{13}C NMR spectroscopies. The ^1H NMR spectra appeared within the standard chemical shift window (0−10 ppm), with two sets of aryl peaks, ranging from 7.34 and 6.19 ppm for **1-NMe_2** to 7.15 and 6.88 ppm for **1-Cl**. The resonance of methyl protons of $N(SiMe_3)_2$ ligands appeared as two peaks in the ^1H NMR spectra for **1-R** complexes due to hindered rotation along the U−N bond. These peaks ranged from 0.77 and 0.72 ppm for **1-NMe_2** to 0.68 and 0.65 ppm for **1-Cl**. Overall, ^1H chemical shifts of **1-R** complexes agreed well with those reported for the parent **1-H**, which had two aryl peaks at 7.44 and 6.95 ppm,

DOI: 10.1021/acs.inorgchem.8b03175
Inorg. Chem. 2019, 58, 4152−4163

and $N(SiMe_3)_2$ ligand resonances were coincident at 0.70 ppm.[10]

The ^{13}C NMR spectra for the **1-R** complexes showed abnormal shifts for atoms in close contact with the uranium center. The acetylide β-carbon atoms (those not bound to the uranium center), U−C≡*C*−Ar, were shifted downfield only moderately (103.3−103.9 ppm) when compared with the ^{13}C chemical shifts in the free alkynes H−C≡C−Ar (82.7−85.3 ppm, cf. Figures S12−S17 in the Supporting Information).[47,48] The acetylide carbons directly bound to the uranium center, however, were high-frequency shifted by about 325 ppm from their ^{13}C chemical shifts in the corresponding free alkynes! Specifically, the H−C≡C−Ar carbon resonances ranged from 75.6 to 78.7 ppm for the $-NMe_2$ and −Cl substituted (phenyl)acetylenes (cf. Figures S12−S17 in Supporting Information), while ^{13}C chemical shifts for the U−*C*≡C−Ar carbon atoms were observed in the range of 409.7 to 392.1 ppm for **1-NMe$_2$** and **1-Cl**, respectively (Figure 2).

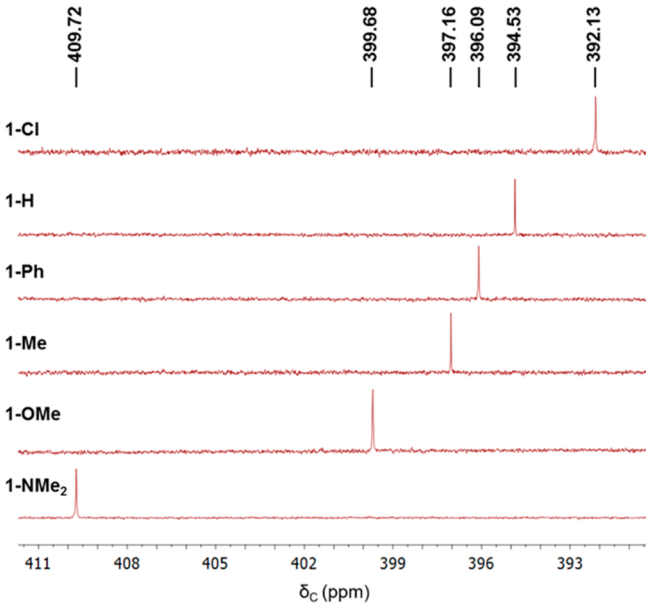

Figure 2. Excerpt of the ^{13}C NMR spectra of **1-R** (R = NMe_2, OMe, Me, Ph, H, Cl) complexes in benzene-d_6 showing the chemical shifts (in ppm vs TMS) of the U−C acetylide carbon atom.

In keeping with expectations, the chemical shift of the primary carbon in free alkynes, H−*C*≡C−Ar, correlated linearly (R^2 = 0.900) with the Hammett parameters of the *para* substituent (Figure 3, top), where the conventional trend in which electron donating groups shield and electron withdrawing groups deshield nearby groups was observed. The ^{13}C chemical shifts of the uranium-bound carbon, U−*C*≡C−Ar, in **1-R** complexes also correlated well with the Hammett parameters (σ_p) for the *para* substituents (with R^2 = 0.985), but in the opposite direction (negative slope) as compared to free alkynes (Figure 3, bottom).[49] Namely, the substituents with increased electron-donating strength (Ph < Me < OMe < NMe_2) shifted the acetylide carbon, U−*C*≡C−Ar, further downfield as compared to **1-H**, despite somewhat more negative charge on the acetylide carbon atom (see natural population analysis and discussion below). To rationalize this observation and to understand the electronic structure of **1-R** complexes more thoroughly, we studied their structures and

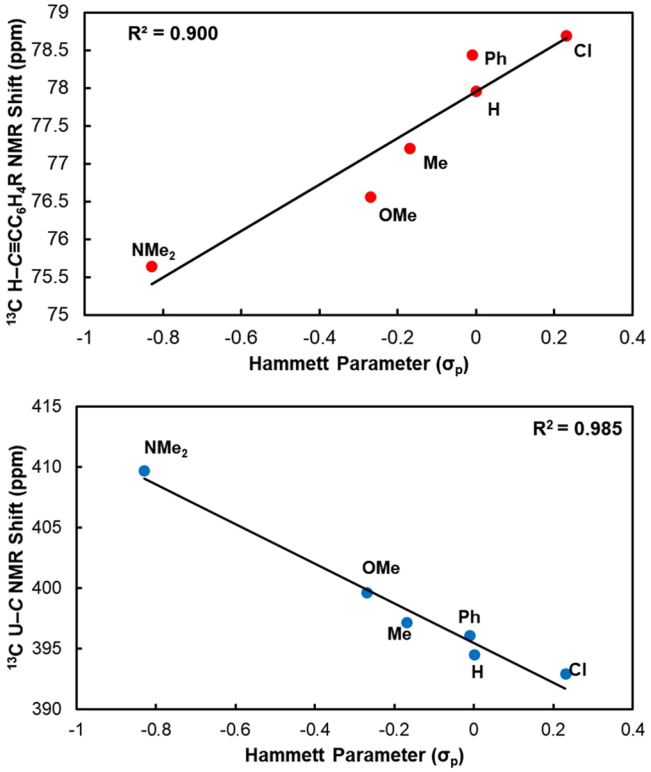

Figure 3. Correlation of the ^{13}C chemical shifts of primary acetylide carbon atoms in the free alkynes, H−C≡C−C_6H_4−R (R = NMe_2, OMe, Me, H, Ph, Cl; top), and uranium complexes (**1-R**), U−C≡C−C_6H_4−R (R = NMe_2, OMe, Me, H, Ph, Cl) (bottom), with the Hammett parameter (σ_p).

U−C bonding experimentally and computationally using DFT calculations.

X-Ray Studies and Correlations of U−C Bond Lengths with ^{13}C NMR Shifts. We structurally characterized the series of uranium(VI) complexes, **1-R** (R = NMe_2, OMe, Me, Ph, Cl), and compared these substituted derivatives to **1-H** (Figure 4, Table 1).[10] The U−O and U−N bond lengths for **1-H** were 1.811(10) and 2.201(6) Å, respectively, and were statistically indistinguishable across the **1-R** series. The O−U−C bond angle varied by approximately 3° within the series; complexes with electron donating (NMe_2) and withdrawing (Cl) substituents both had near linear O−U−C angles of 178.91(14) and 179.20(9)°. However, **1-H** had a slightly bent O−U−C bond angle of 177.2(7)°. The U−C−C bond angle was noticeably more bent for **1-NMe$_2$** at 173.4(4)°, while the other derivatives had a more linear average U−C−C bond angle of 176.2(11)°. These variations are, however, proposed to result from different crystal packing forces in the solid-state structures.

The U(1)−C(19) bond lengths were of special interest to us because we had hypothesized that the downfield shift of the acetylide carbons, U−C≡C−Ar, in complexes with electron-donating substituents was due to shortened U−C bonds for these complexes. Although the X-ray data were not of sufficient quality to distinguish between the majority of the U−C bond lengths, a statistical difference was observed for the U−C bond length of **1-NMe$_2$**, which was short (2.279(4) Å) in comparison with the U−C bond lengths of **1-OMe**, **1-Ph**, **1-H**, and **1-Cl**, which were 2.316(2), 2.303(2), 2.337(14), and 2.315(3) Å, respectively. However, when the ^{13}C NMR

DOI: 10.1021/acs.inorgchem.8b03175
Inorg. Chem. 2019, 58, 4152−4163

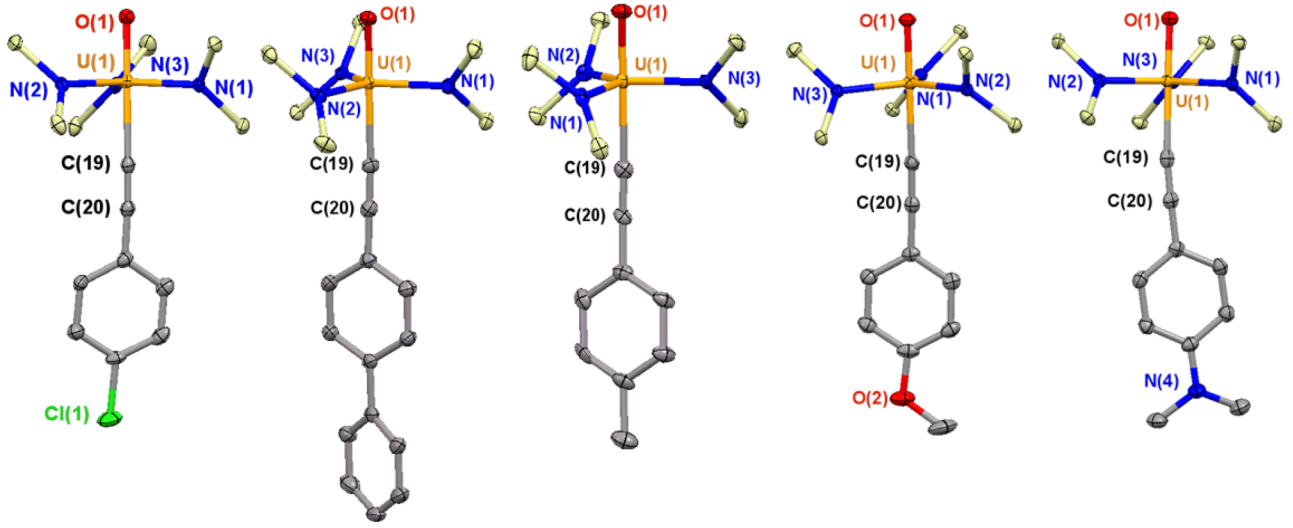

Figure 4. Thermal ellipsoid plots of **1-R** (R = NMe_2, OMe, Me, Ph, Cl) at 50% probability. All hydrogen atoms and amide methyl groups are omitted for clarity.

Table 1. Selected X-Ray Bond Lengths (Å) and Angles (deg) for U(VI)−Acetylide Complexes 1-R (R = NMe_2, OMe, Me, Ph, H, Cl)[a,10]

	bond lengths (Å)				bond angles (deg)	
R	U−O	U−$N_{avg.}$	U−C	C≡C	O−U−C	U−C−C
NMe_2	1.819(3)	2.209(3)	2.279(4)	1.227(6)	178.91(14)	173.4(4)
OMe	1.8121(15)	2.2072(17)	2.316(2)	1.209(3)	179.89(8)	176.18(19)
Me	1.811(7)	2.208(8)	2.313(11)	1.208(14)	179.3(4)	176.0(9)
Ph	1.8013(16)	2.2041(18)	2.303(2)	1.217(3)	179.73(8)	176.7(2)
H	1.811(10)	2.201(6)	2.337(14)	1.209(1)	177.2(7)	176.9(14)
Cl	1.7989(18)	2.201(2)	2.315(3)	1.217(4)	179.20(9)	175.3(2)

[a]The crystal structure of **1-H** was previously reported.

Table 2. Optimized U−C Bond Lengths, Corresponding QTAIM Delocalization Indices (DI) and Wiberg Bond Orders (WBI), NPA Atomic Charges (q), ^{13}C NMR Shielding Contributions (σ) and Total Shifts (δ) Calculated for the Uranium-Bound Carbon Atoms in 1-R Complexes[a,b,c]

R	d(U−C) [Å]	DI(U−C)	WBI(U−C)	q(C)	σ^{dia} [ppm]	σ^{para} [ppm]	σ^{SO} [ppm]	$\delta_{calcd.}(^{13}C)$ [ppm]	$\delta_{expt.}(^{13}C)$ [ppm]
NMe_2	2.281	0.796	0.903	−0.297	268.8	−291.7	−214.6	408.8	409.7
OMe	2.295	0.775	0.879	−0.282	269.0	−284.9	−212.8	400.0	399.7
Me	2.302	0.765	0.868	−0.274	268.5	−282.6	−212.4	397.8	397.0
Ph	2.302	0.759	0.867	−0.261	268.1	−281.7	−212.2	397.1	396.1
H	2.307	0.753	0.860	−0.267	268.5	−281.0	−210.7	394.5	394.5
Cl	2.31.2	0.746	0.851	−0.265	269.2	−280.7	−208.7	391.5	392.1
CN	2.328	0.724	0.829	−0.241	268.8	−278.9	−205.4	386.8	
NO_2	2.330	0.723	0.828	−0.220	268.0	−277.5	−205.7	386.5	

[a]See Computational Details. [b]Chemical shieldings/shifts calculated at the 2c-ZORA(SO)/PBE0-40HF/TZ2P level. Data computed at the 2c-ZORA(SO)/PBE0-15HF/TZ2P level, including XC response kernel, are listed in Table S6 in the Supporting Information and are of the same quality as those reported here. [c]Experimental ^{13}C NMR shifts (in ppm vs. TMS) are given as well.

resonances of the acetylide ligand were plotted against the experimental U−C bond lengths, a poor correlation (R^2 = 0.630) was obtained, presumably due to the large standard deviations on the experimental U−C bond lengths (cf. Figure S21 in the Supporting Information).

DFT Computed Electronic Structures and ^{13}C NMR Chemical Shifts. To ascertain that the difference we observed in the U−C bond length of **1-NMe_2** compared with the other **1-R** complexes was not the result of crystal packing forces, we carried out DFT structure optimizations and electronic structure analysis on the series of **1-R** complexes. A hybrid DFT method was employed with the B3LYP functional along with Grimme's D3 dispersion forces, using a 60 electron effective core potential applied to uranium, and the def2-TZVP basis set for all other atoms. In addition, we also computed ^{13}C NMR shifts for uranium-bound acetylide carbon atoms at the two-component ZORA relativistic level, including spin−orbit coupling (see Computational Details).

The computed bond lengths agreed well with the experimental bond distances and showed trends that were too subtle to observe in the experimental X-ray data (cf. Table S2 in the Supporting Information). Besides the experimentally characterized **1-R** complexes (R = NMe_2, OMe, Me, Ph, H, Cl), we also considered in our theoretical investigations

DOI: 10.1021/acs.inorgchem.8b03175
Inorg. Chem. 2019, 58, 4152−4163

complexes with cyano (**1-CN**) and nitro (**1-NO$_2$**) groups located in the *para* position of the aryl(acetylide) ring, which were not synthetically accessible in our hands, to study the trends for a wider set of substituents. Additionally, computed ^{13}C chemical shifts of the uranium-bound carbon agreed excellently with experimental ^{13}C chemical shift values (R^2 = 0.986; cf. Table 2 and Figure S22 in the Supporting Information).

When examining the computed bond distances in the entire series (cf. Table 2 and Table S2 in the Supporting Information), a trend was observed in which the U−C bond shortened as electron donating ability of the *para* substituent increased. At the most extreme ends of the series **1-NMe$_2$** had a computed U−C bond length of 2.281 Å, while **1-Cl** and **1-NO$_2$** had computed bond lengths of 2.312 and 2.330 Å, respectively. The excellent linear correlation between experimental and computed ^{13}C NMR shifts with DFT calculated U−C bond lengths (R^2 > 0.970; Figure 5), as well as with

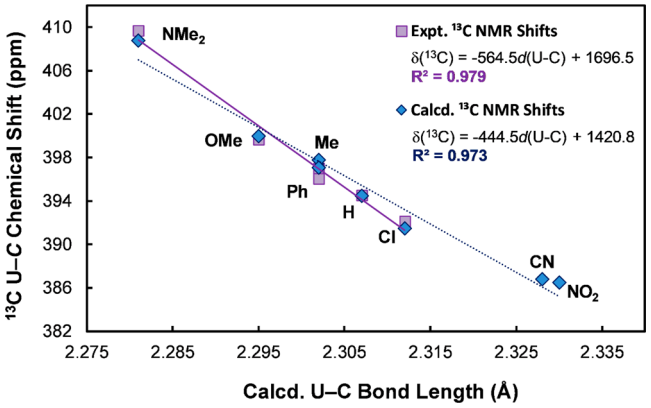

Figure 5. Experimental and calculated ^{13}C NMR chemical shifts of the U−C acetylide carbon atoms (in ppm vs TMS) plotted versus the calculated U−C bond lengths (Å) for **1-R** complexes (cf. Table 2 for numerical data).

Hammett parameters of the *para* substituent (Figure 3, bottom), supported our hypothesis that the U−C bond shortened with increased electron donation from the substituted (aryl)acetylide ligand. This in turn affected the U−C bond covalency and thus the orbital interaction of the ligand with the uranium(VI) center, as evident from Wiberg bond orders and QTAIM topological analysis via U−C delocalization indices, DI(U−C) (cf. Table 2 and Tables S3 and S5 in the Supporting Information), and led to higher frequency shifts for complexes with the electron-donating substituents when compared to **1-H**. Correlations of experimental and computed U−C carbon chemical shifts with the U−C bond covalency, represented by delocalization indices and Wiberg bond orders, respectively, are depicted in Figure 6, showing an almost perfect linear behavior.

Analysis of computed ^{13}C shielding showed that the extreme downfield shifts of U−C≡C−Ar carbon atoms can be attributed to large paramagnetic (σ^{para}) and relativistic spin−orbit (σ^{SO}) deshielding contributions (Table 2), both associated with extensive metal participation in the U−C bonding along with low-lying unoccupied orbitals with predominant U(5f) character.[36,37] According to NLMO hybridization analysis (cf. Table S4 in the Supporting Information), U−C bonds of **1-R** complexes possessed about a 28−29% uranium contribution with 60−62% f-character,

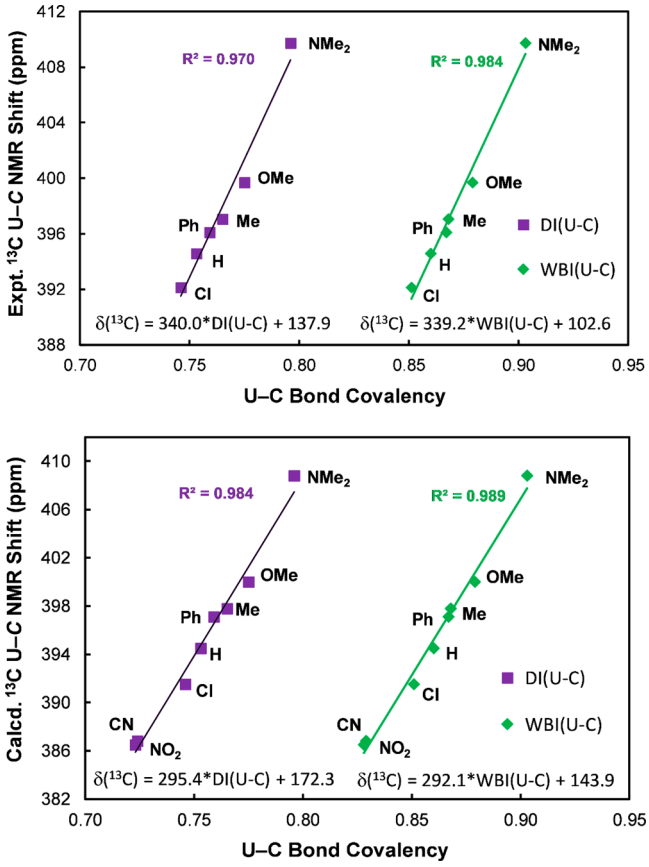

Figure 6. Experimental (top) and calculated (bottom) ^{13}C NMR shifts of the U−C acetylide carbon (in ppm vs TMS) in **1-R** complexes plotted versus the U−C bond covalency represented by QTAIM delocalization indices, DI(U−C), and Wiberg bond orders, WBI(U−C) (see Table 2 for numerical data).

resulting in an overall 17% of U(5f) contribution to the U−C bonds. Moreover, the acetylide carbon atoms were sp-hybridized with large C(2s) character in the σ(U−C) bonding, which effectively mediated the heavy-atom induced spin−orbit (SO) effects to a ligand atom through the Fermi-contact-type mechanism.[50,36,37] The σ^{SO} contributions in **1-R** were about 50 ppm larger as compared to an analogous U(O)Me[N(SiMe$_3$)$_2$]$_3$ complex with an sp^3 hybridized methyl carbon atom, which displayed a U−Me ^{13}C NMR resonance at 301 ppm.[10] We note in passing that this finding is consistent with previous theoretical studies on HALA (heavy-atom-effects on the light-atom) "spin-orbit" shifts in transition-metal and actinide complexes.[34,36,50−56] Similarly, owing to the large hydrogen 1s-orbital contribution to the An−H bonding, as-yet elusive uranium(VI) hydrides were predicted to exhibit giant downfield ^{1}H hydride shifts between +30 ppm and more than +200 ppm.[36,37]

From Table 2, it was clear that the diamagnetic (σ^{dia}) term remained almost constant and the changes in $\delta(^{13}C)$ shifts across the series were dictated by σ^{para} and σ^{SO} contributions, which were roughly parallel along the series. Interestingly, artificial elongation of U−C bonds in **1-NMe$_2$** or **1-H** complexes by 0.03 Å led to moderate downfield shifts (+ 3 ppm) of $\delta(^{13}C)$ values, despite the expected decrease of U−C bond covalency—thus in opposite direction as observed across the **1-R** series with optimized U−C bond lengths (cf. Table S8 in Supporting Information). This observation demonstrated

DOI: 10.1021/acs.inorgchem.8b03175
Inorg. Chem. 2019, 58, 4152−4163

that not only U−C bond lengths and metal−ligand covalencies but also corresponding atomic charges and, in particular, energy levels of relevant magnetically active occupied and vacant orbitals should be considered when explaining the trends thoroughly.[57]

According to Ramsey's formula for σ^{para},[58−60] the large paramagnetic deshielding contributions of the U(VI)-bound carbon in **1-R** complexes can be rationalized by its short distance to the uranium center (accompanied with a large U−C bond covalency) and by symmetry-allowed couplings between the occupied molecular orbitals and low-lying virtual orbitals, with predominant uranium 5f character, involved in the perturbation-theoretical treatment of chemical shieldings.[61−63] Not surprisingly, ^{13}C NMR shifts of the U(VI)-bound acetylide carbon atoms were found to correlate with the reciprocal of the energy of the LUMO (cf. Figure S23 in the Supporting Information), which is basically a uranium-centered f-orbital within the entire series (Figure 7). The

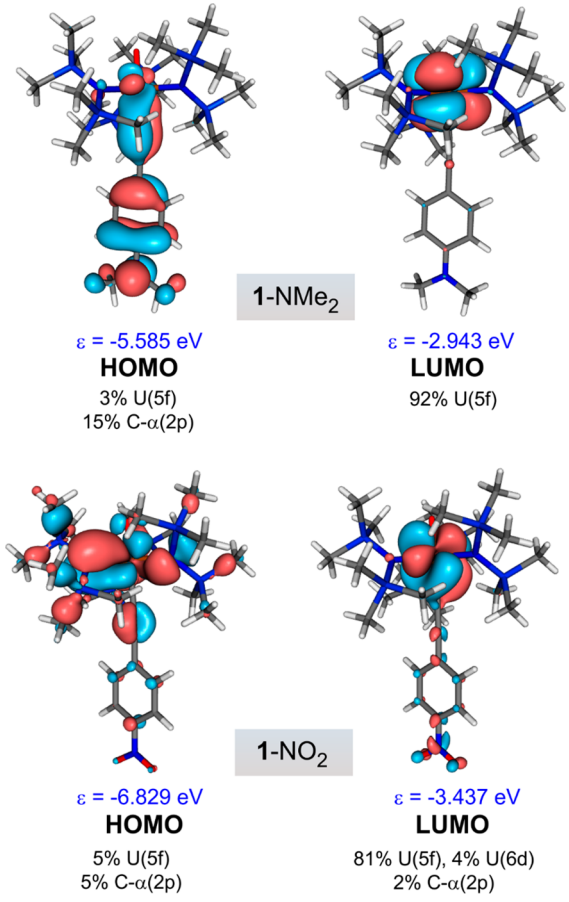

Figure 7. Frontier molecular orbitals (isosurface plots, ±0.03 au) of extreme cases, **1-NMe$_2$** and **1-NO$_2$**, with an electron-donating (NMe_2) and electron-withdrawing (NO_2) *para* substituent, respectively. Orbital energies and composition from Mulliken population analysis, as obtained at the B3LYP-D3(BJ)/def2-TZVP/ECP level, are indicated below corresponding MOs.

magnetic field-induced mixing of the ground state with low-lying (thermally inaccessible) paramagnetic excited states is also confirmed experimentally by SQUID measurements of selected **1-R** complexes (R = NMe_2, Cl). These measurements revealed a temperature independent paramagnetism (TIP) of the compounds, evident from small positive slopes in the temperature dependent χT data (cf. Figures S18−S20 in the Supporting Information), despite the ground-state singlet (f^0) electronic configuration of U(VI) ion.

Similarly, low-lying vacant d orbitals are responsible for TIP behavior of some high-oxidation-state transition-metal d^0 complexes ("closed-shell" tetraoxo anions and oxides of Cr(VI), Mn(VII), and Ru(VIII) being the most illustrative and well-studied examples[64,65]) and influence their ligand NMR shifts,[66−68] which are often shifted notably downfield as observed here for uranium(VI) f^0 systems.

Electrochemistry. Compounds **1-R** (R = NMe_2, OMe, Me, Ph, H, Cl) were characterized by solution electrochemistry (Figure 8, top). These compounds were not stable for an extended time under electrochemical conditions. However,

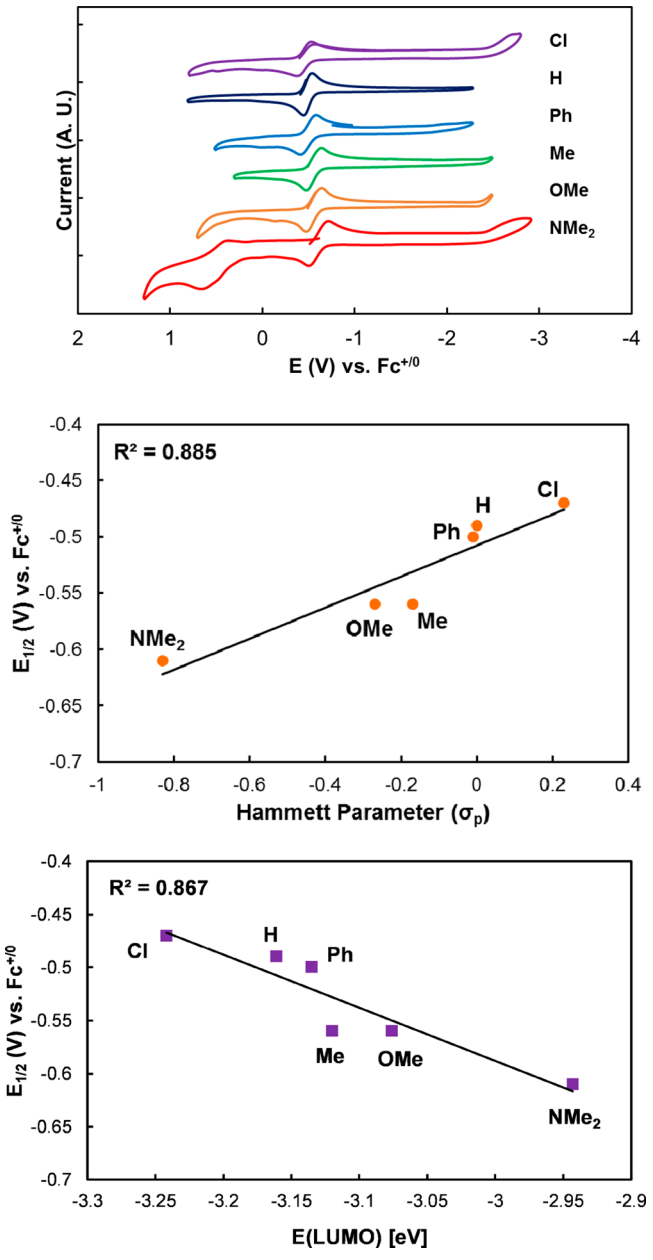

Figure 8. Cyclic voltammograms of **1-R** complexes in THF with 0.1 M [^{n}Bu$_4$N][PF$_6$] supporting electrolyte at a scan rate of 250 mV/s (top). Correlation of $E_{1/2}$ for the U(VI)/U(V) couple with Hammett parameter, σ_p (middle), and energy of LUMO orbitals (bottom).

DOI: 10.1021/acs.inorgchem.8b03175
Inorg. Chem. 2019, 58, 4152−4163

cyclic voltammograms were collected in THF with 0.1 M [^{n}Bu$_4$N][PF$_6$] supporting electrolyte. Redox potentials of the U(VI)/U(V) couple ranged from −0.47 to −0.61 V (vs Fc$^{+/0}$) for **1-Cl** and **1-NMe$_2$**, respectively (Table S1). This 140 mV range of $E_{1/2}$ values for the studied **1-R** complexes showed a reasonable correlation with the Hammett parameters of the *para* substituents (R^2 = 0.885; Figure 8, middle) as well as with the energies of the LUMO (R^2 = 0.867; Figure 8, bottom), which is primarily a U(5f)-centered vacant orbital (cf. Figure 7), that is active in the U(VI)/U(V) redox process. The stabilization of the +6 oxidation state, as indicated by the negative shift of the $E_{1/2}$ for the U(VI/V) couple, for **1-NMe$_2$** further indicated that the electron-donating substituent, NMe$_2$, was able to increase the electron density at the uranium center by electron donation through the acetylide ligand. In the case of **1-NMe$_2$**, we also detected an oxidation wave, attributed to the amine$^{+/0}$ redox process with an $E_{1/2}$ value of +0.52 V (see Figure 7 for HOMO of **1-NMe$_2$**).

Previously, other structurally related series of high-valent uranium complexes have been synthesized and characterized electrochemically. For example, Kiplinger and Graves developed a series of uranium(V)-imido halide complexes of the general formula $(C_5Me_5)_2U^V(=NAr)X$ (Ar = 2,6-^{i}Pr$_2$−C$_6$H$_3$), where X = F, Cl, Br, I, OTf, SPh, CCPh, NPh$_2$, OPh, Me, and NCPh$_2$. Within this series of compounds, the halide compounds exhibited $E_{1/2}$ values for the U(VI)/U(V) couple ranging from −0.19 to +0.11 V versus Fc$^{+/0}$, for F and I ligands, respectively.[69,70] In this series the halide ligands were directly bound to the uranium center and shifted the redox potential of U(VI)/U(V) couple by 300 mV, so it was noteworthy that in our complexes a distal aryl substituent changed the U(VI)/U(V) couple by 140 mV.

CONCLUSIONS

We have synthesized a series of uranium(VI) (aryl)acetylide complexes of the general formula $U^{VI}(O)(C{\equiv}C{-}C_6H_4{-}R)[N(SiMe_3)_2]_3$ (**1-R**), with R = NMe$_2$, OMe, Me, Ph, H, Cl. Correlation of structural data with the Hammett parameters of the *para* substituent showed that electron-donating or withdrawing groups shortened and elongated the U−C bond, respectively. This bond shortening along with electron density accumulation in the U−C bonding region led to moderate deshielding of the U−C≡C−Ar acetylide ^{13}C NMR resonance, which thus serves as a sensitive probe of the actinide-carbon bond covalency and provides an insight into the charge redistribution within the title complexes. SQUID magnetometry revealed the Van Vleck temperature independent paramagnetism (TIP) of the studied U(VI) complexes, suggesting a magnetic-field induced mixing of the diamagnetic (closed-shell) ground-state (f^0) of the U(VI) ion with low-lying paramagnetic excited states.

Electrochemical data confirmed that the *para* substituent on the (aryl)acetylide ligand affected the electron density at the U−C bond as well as the energy of frontier orbitals. Redox potentials ($E_{1/2}$) of the U(VI)/U(V) couple within the studied **1-R** series showed a range of 140 mV and correlated well with the Hammett parameters of the substituents and calculated energies of the LUMO.

EXPERIMENTAL SECTION

General Methods. All reactions and manipulations were performed under an inert atmosphere (N$_2$) using standard Schlenk techniques or in a Vacuum Atmospheres, Inc. Nexus II drybox equipped with a molecular sieves 13X/Q5 Cu-0226S catalyst purifier system. Glassware was oven-dried overnight at 150 °C prior to use. ^{1}H and ^{13}C{^{1}H} NMR spectra were obtained on a Bruker DRX-500 Fourier transform NMR spectrometer operating at 500 MHz (^{1}H) and 126 MHz (^{13}C). Chemical shifts were recorded in units of parts per million (ppm) downfield from residual proteo solvent peaks (benzene-d_6, δ_H = 7.16 ppm, δ_C = 128.06 ppm). Elemental analyses were performed at Complete Analysis Laboratories, Inc. (Parsippany, NJ) or on a Costech ECS 4010 analyzer at the Earth and Environmental Science department of the University of Pennsylvania. The infrared spectra were obtained from 400−4000 cm^{-1} using a PerkinElmer 1600 series infrared spectrometer.

Materials. Tetrahydrofuran, Et$_2$O, CH$_2$Cl$_2$, hexanes, pentane, and toluene were purchased from Fisher Scientific. These solvents were sparged for 20 min with dry argon and dried using a commercial two-column solvent purification system comprising columns packed with Q5 reactant and neutral alumina, respectively (for hexanes and pentane), or two columns of neutral alumina (for THF, Et$_2$O, and CH$_2$Cl$_2$). All solvents were stored over 3 Å molecular sieves. Benzene-d_6 was purchased from Cambridge Isotope Laboratories, Inc. and stored over a potassium mirror overnight prior to use. Starting materials: $UI_3(THF)_4$,[71] $U[N(SiMe_3)_2]_3$,[72] and **1-H**[10] were prepared according to the reported procedures. Substituted copper(I) acetylide compounds were prepared according to the literature procedure to prepare copper(I) phenyl acetylide.[73]

Electrochemistry. Voltammetry experiments (CV, DPV) were performed using a CH Instruments 620D Electrochemical Analyzer/Workstation, and the data were processed using CHI software v9.24. All experiments were performed in an N$_2$ atmosphere drybox using electrochemical cells that consisted of a 4 mL vial, glassy carbon working electrode, a platinum wire counter electrode, and a silver wire plated with AgCl as a quasi-reference electrode. The quasi-reference electrode was prepared by dipping a length of silver wire in concentrated hydrochloric acid. The working electrode surfaces were polished prior to each set of experiments. Potentials were reported versus ferrocene, which was added as an internal standard for calibration at the end of each run. Solutions employed during these studies were ∼3 mM in analyte and 100 mM in [^{n}Bu$_4$N][PF$_6$] in 2 mL of THF. All data were collected in a positive-feedback IR compensation mode.

X-ray Crystallography. X-ray intensity data were collected on a Bruker APEXII CCD area detector employing graphite-monochromated Mo Kα radiation (λ = 0.71073 Å) at a temperature of 100(1) K. In all cases, rotation frames were integrated using SAINT,[74] producing a listing of unaveraged F^2 and $\sigma(F^2)$ values which were then passed to the SHELXTL[75] program package for further processing and structure solution. The intensity data were corrected for Lorentz and polarization effects and for absorption using TWINABS[76] or SADABS.[77] The structures were solved by direct methods (SHELXS-97).[78] Refinement was by full-matrix least-squares based on F^2 using SHELXL-97.[78] All reflections were used during refinements. Non-hydrogen atoms were refined anisotropically, and hydrogen atoms were refined using a riding model.

Computational Details. All structures were fully optimized without symmetry restrictions at the B3LYP level of theory,[79−81] including an atom-pairwise correction for dispersion forces via Grimme's D3 model with Becke-Johnson (BJ) damping[82,83] in the Turbomole program.[84] A quasirelativistic energy-consistent small-core pseudopotential (with 60 core electrons)[85] was used for the uranium center, together with a (14s13p10d8f1g)/[10s9p5d4f1g] Gaussian-type orbital valence basis set, while ligand atoms were treated with an all-electron def2-TZVP basis set.[86] Relativistic all-electron DFT calculations of the nuclear shieldings were performed using the Amsterdam Density Functional (ADF) program suite,[87] employing a user-customized hybrid PBE0 exchange-correlation functional[88−90] with 15% and 40% of Hartree−Fock (exact-exchange, EXX) admixture (denoted as PBE0-15HF and PBE0-40HF, respectively) in conjunction with Slater-type orbital basis sets of triple-ζ doubly polarized (TZ2P) quality and an integration accuracy of 5. Both scalar and spin−orbit relativistic effects were treated by the two-component

DOI: 10.1021/acs.inorgchem.8b03175
Inorg. Chem. 2019, 58, 4152−4163

zeroth-order regular approximation (ZORA).[91−94] The ZORA calculations of NMR shieldings were done by using gauge-including atomic orbitals (GIAOs)[95] with and without the previously neglected terms from the exchange−correlation (XC) response kernel.[36,37] The computed ^{13}C nuclear shieldings were converted to chemical shifts (δ, in ppm) relative to the shieldings of tetramethylsilane (TMS), considering **1-H** as a secondary standard, with $\delta(^{13}C)$ = 394.5 ppm.

We note here that computed ligand NMR shifts in actinide complexes are particularly sensitive to the DFT method used. Our choice of functionals (PBE0-40HF and PBE0-15HF/XC) is based on the previous benchmark studies on ^{13}C NMR shifts in actinide complexes.[34,36,37] While the PBE0-40HF hybrid functional with missing XC kernel in the older ADF implementations was found to work very well (due to a fortuitous compensation between missing XC kernel and too large amount of Hartree−Fock exact exchange), a proper kernel treatment in two-component ZORA calculations required lower EXX admixtures, with the optimal value of around 15% for systems with extremely large spin−orbit-induced NMR shifts.[37]

Evaluation of Wiberg bond indices (WBI), natural population analyses (NPA), and analysis of natural localized molecular orbitals (NLMOs)[96] were carried out at the B3LYP/def2-TZVP/ECP level using the NBO6 code,[97] interfaced with Gaussian 09.[98] Bader's quantum theory of atoms-in-molecules (QTAIM)[99−101] analyses of the Kohn−Sham wave functions were performed at the same level using the Multiwfn program.[102]

Synthesis of 1-NMe$_2$. To a stirred solution of U[N(SiMe$_3$)$_2$]$_3$ (200 mg, 0.28 mmol, 1.0 equiv) in Et$_2$O was added [(4-(dimethylamino)phenyl)ethynyl]copper (115 mg, 0.56 mmol, 2.0 equiv). The mixture was stirred for 2 h and filtered over Celite. *N*-Methylmorpholine *N*-oxide (33 mg, 0.28 mmol, 1.0 equiv) was added, resulting in an immediate color change to dark red. After being stirred for 1 h, volatiles were removed under reduced pressure. The resulting black residue was extracted with hexanes, filtered over Celite, and stored at −21 °C to give black crystals. Yield: 68 mg, 0.08 mmol, 28%. ^{1}H NMR (benzene-d_6): 7.34 (d, 2H), 6.19 (d, 2H), 2.43 (s, 6H), 0.77 (s, 27H), 0.72 (s, 27H). ^{13}C NMR (benzene-d_6): 409.72 (U−C≡C−R), 151.02 (Ar), 132.96 (Ar), 112.89 (Ar), 103.40 (U−C≡*C*−R), 39.12 (NMe$_2$), 6.93 (SiMe$_3$). IR (KBr): 2961 (s), 2899 (w), 2799 (w), 2023 (m, *C*≡*C*), 1607 (m), 1520 (m), 1457 (w), 1358 (w), 1258 (s), 1186 (m), 1117 (w), 1104 (w), 936 (s), 879 (m), 850 (s), 683 (w), 655 (w), 612 (w). Elemental analysis found (calculated) for $C_{28}H_{64}N_4OSi_6U$: C, 38.12 (38.24); H, 7.32 (7.34); N, 6.17 (6.37).

Synthesis of 1-OMe. To a stirred solution of U[N(SiMe$_3$)$_2$]$_3$ (500 mg, 0.70 mmol, 1.0 equiv) in Et$_2$O was added [4-methoxyphenyl)ethynyl]copper (270 mg, 1.39 mmol, 2.0 equiv). The mixture was stirred for 2 h, and volatiles were removed under reduced pressure. The residue was extracted with hexanes and filtered over Celite, and volatiles were removed under reduced pressure. The residue was redissolved in Et$_2$O, and *N*-methylmorpholine *N*-oxide (81 mg, 0.70 mmol, 1.0 equiv) was added, resulting in an immediate color change to dark red. After being stirred for 1 h, volatiles were removed under reduced pressure. The resulting black residue was extracted with hexanes, filtered over Celite, and stored at −21 °C. Yield: 35 mg, 0.04 mmol, 6%. ^{1}H NMR (benzene-d_6): 7.35 (d, 2H), 6.53 (d, 2H), 3.13 (s, 3H), 0.72 (s, 27H), 0.71 (s, 27H). ^{13}C NMR (benzene-d_6): 399.68 (U−C≡C−R), 161.32 (Ar), 133.11 (Ar), 115.11 (Ar), 103.37 (U−C≡C−R), 54.76 (OMe), 6.97 (SiMe$_3$). IR (KBr): 2957 (s), 2902 (m), 2056 (m, C≡C), 1603 (m), 1505 (m), 1463 (m), 1442 (m), 1295 (w), 1261 (s), 1181 (m), 1169 (w), 1108 (m), 1092 (w), 1030 (w), 935 (s), 883 (s), 842 (s), 774 (m), 656 (w), 615 (w). Elemental analysis found (calculated) for $C_{27}H_{61}N_3O_2Si_6U$: C, 37.75 (37.43); H, 6.63 (7.10); N, 4.91 (4.85).

Synthesis of 1-Me. To a stirred solution of U[N(SiMe$_3$)$_2$]$_3$ (500 mg, 0.70 mmol, 1.0 equiv) in Et$_2$O was added (*p*-tolylethynyl)copper (249 mg, 1.39 mmol, 2.0 equiv). The mixture was stirred for 2 h, and volatiles were removed under reduced pressure. The residue was extracted with hexanes and filtered over Celite, and volatiles were removed under reduced pressure. The residue was redissolved in Et$_2$O and *N*-methylmorpholine *N*-oxide (81 mg, 0.70 mmol, 1.0 equiv) was added, resulting in an immediate color change to dark red. After being stirred for 1 h, volatiles were removed under reduced pressure. The resulting black residue was extracted with hexanes, filtered over Celite, and crytallized at −21 °C to yield black crystals. Yield: 55 mg, 0.06 mmol, 9%. ^{1}H NMR (benzene-d_6): 7.37 (d, 2H), 6.79 (d, 2H), 1.95 (s, 3H), 0.71 (s, 27H), 0.70 (s, 27H). ^{13}C NMR (benzene-d_6): 397.04 (U−C≡C−R), 140.05 (Ar), 131.38 (Ar), 129.95 (Ar), 116.68 (Ar), 103.57 (U−C≡*C*−R), 21.32 (Me), 6.97 (SiMe$_3$). IR (KBr): 2952 (m), 2897 (w), 2059 (m, *C*≡*C*), 1504 (m), 1248 (s), 1178 (w), 1039 (w), 873 (s), 844 (s), 773 (m), 681 (w), 653 (s), 620 (s). Elemental analysis found (calculated) for $C_{27}H_{61}N_3OSi_6U$: C, 37.81 (38.14); H, 6.82 (7.23); N, 5.02 (4.94).

Synthesis of 1-Ph. To a stirred solution of U[N(SiMe$_3$)$_2$]$_3$ (750 mg, 1.04 mmol, 1.0 equiv) in Et$_2$O was added [(1,1′-biphenyl)-4-ethynyl]copper (502 mg, 2.08 mmol, 2.0 equiv). The mixture was stirred for 2 h, and volatiles were removed under reduced pressure. The residue was extracted with hexanes and filtered over Celite, and volatiles were removed under reduced pressure. The residue was redissolved in Et$_2$O, and *N*-methylmorpholine *N*-oxide (122, 1.04 mmol, 1.0 equiv) was added, resulting in an immediate color change to dark red. After being stirred for 1 h, volatiles were removed under reduced pressure. The resulting black residue was extracted with hexanes, filtered over Celite, and stored at −21 °C. Yield: 30 mg, 0.03 mmol, 3%. ^{1}H NMR (benzene-d_6): 7.46 (d, 2H), 7.29 (d, 2H), 7.25 (d, 2H), 7.14 (d, 2H), 7.08 (t, 1H), 0.71 (s, 27H), 0.68 (s, 27H). ^{13}C NMR (benzene-d_6): 396.09 (U−C≡C−R), 142.63 (Ar), 140.35 (Ar), 131.84 (Ar), 129.14 (Ar), 127.35 (Ar), 118.62 (Ar), 103.90 (U−C≡*C*−R), 7.00 (SiMe$_3$). IR (KBr): 2957 (s), 2897 (m), 2797 (m), 2698 (w), 2058 (m, *C*≡*C*), 1600 (w), 1484 (m), 1455 (m), 1404 (w), 1288 (w), 1249 (s), 1183 (m), 1145 (w), 1103 (m), 1064 (w), 957 (s), 939 (s), 841 (s), 762 (m), 686 (w), 654 (w), 612 (w). Elemental analysis found (calculated) for $C_{32}H_{63}N_3OSi_6U$: C 42.85 (42.12), H 6.44 (6.96), N 4.45 (4.61). We attempted elemental analysis on two independently prepared samples. However, the experimental carbon value differed from the calculated by 0.73%.

Synthesis of 1-Cl. To a stirred solution of U[N(SiMe$_3$)$_2$]$_3$ (200 mg, 0.28 mmol, 1.0 eqiv) in Et$_2$O was added [(4-chlorophenyl)-ethynyl]copper (110 mg, 0.56 mmol, 2.0 equiv). The mixture was stirred for 2 h and filtered over Celite. *N*-Methylmorpholine *N*-oxide (33 mg, 0.28 mmol, 1.0 equiv) was added, resulting in an immediate color change to dark red. After being stirred for 1 h, volatiles were removed under reduced pressure. The resulting black residue was extracted with hexanes, filtered over Celite, and stored at −21 °C to give black crystals. Yield: 45 mg, 0.05 mmol, 18%. ^{1}H NMR (benzene-d_6): 7.15 (d, 2H), 6.88 (d, 2H), 0.68 (s, 27H), 0.65 (s, 27H). ^{13}C NMR (benzene-d_6): 392.13 (U−C≡C−R), 135.75 (Ar), 132.27 (Ar), 129.60 (Ar), 118.83 (Ar), 103.80 (U−C≡*C*−R), 7.00 (SiMe$_3$). IR (KBr): 2965 (s), 2900 (m), 2798 (m), 2698 (w), 2065 (m, C≡C), 1590 (w), 1486 (m), 1457 (m), 1256 (s), 1184 (m), 1146 (w), 1094 (w), 939 (s), 844 (s), 678 (w), 620 (w). Elemental analysis found (calculated) for $C_{26}H_{58}ClN_3OSi_6U$: C, 35.74 (35.86); H, 6.58 (6.71); N, 4.79 (4.83).

■ ASSOCIATED CONTENT

Supporting Information

The Supporting Information is available free of charge on the ACS Publications website at DOI: 10.1021/acs.inorgchem.8b03175.

^{1}H and ^{13}C NMR spectra, field-dependent magnetic data, electrochemical data, and results of quantum-chemical calculations (PDF)

Cartesian coordinates of the DFT-optimized structures (XYZ)

Accession Codes

CCDC 1878398−1878402 contain the supplementary crystallographic data for this paper. These data can be obtained free of charge via www.ccdc.cam.ac.uk/data_request/cif, or by

DOI: 10.1021/acs.inorgchem.8b03175
Inorg. Chem. 2019, 58, 4152−4163

emailing data_request@ccdc.cam.ac.uk, or by contacting The Cambridge Crystallographic Data Centre, 12 Union Road, Cambridge CB2 1EZ, UK; fax: +44 1223 336033.

AUTHOR INFORMATION

Corresponding Authors

*E-mail: peter.hrobarik@uniba.sk.
*E-mail: schelter@sas.upenn.edu.

ORCID

Kimberly C. Mullane: 0000-0003-1085-8038
Peter Hrobárik: 0000-0002-6444-8555
Thibault Cheisson: 0000-0003-4359-5115
Eric J. Schelter: 0000-0002-8143-6206

Notes

The authors declare no competing financial interest.

ACKNOWLEDGMENTS

The authors gratefully acknowledge the U.S. National Science Foundation (CHE-1664928) and University of Pennsylvania for primary support. The authors also gratefully acknowledge the Chemical Sciences, Geosciences, and Biosciences Division, Office of Basic Energy Sciences, Energy Frontier Research Program of the U.S. Department of Energy (Center for Actinide Science and Technology, Florida State University), under Award No. DE-SC0016568 for partial support of K.C.M. and T.C. The Camille and Henry Dreyfus Postdoctoral Program in Environmental Chemistry is acknowledged for a fellowship to T.C. Calculations were performed in the Computing Centre of the Slovak Academy of Sciences using the supercomputing infrastructure acquired in projects ITMS 26230120002 and 26210120002 supported by the Research & Development Operational Programme funded by the ERDF. P.H. acknowledges financial support from the Slovak grant agencies VEGA (grant Nos. 1/0507/17 and 1/0712/18) and APVV (grant No. APVV-17-0324) as well as funding from the European Union's Horizon 2020 research and innovation program under the Marie Skłodowska-Curie Grant No. 752285.

REFERENCES

(1) Gilman, H.; Jones, R. G.; Bindschadler, E.; Blume, D.; Karmas, G.; Martin, G. A.; Nobis, J. F.; Thirtle, J. R.; Yale, H. L.; Yoeman, F. A. Organic Compounds of Uranium. I. 1,3-Dicarbonyl Chelates. *J. Am. Chem. Soc.* **1956**, *78*, 2790−2792.

(2) Zucchini, U.; Giannini, U.; Albizzati, E.; D'Angelo, R. Benzylzirconium Compounds. *J. Chem. Soc. D* **1969**, 1174−1175.

(3) Marks, T. J.; Seyam, A. M.; Kolb, J. R. Synthesis, Chemistry, and Spectroscopy of Some Tris(Pentahapto-Cyclopentadienyl)Uranium-(IV) Alkyl and Aryl Compounds. *J. Am. Chem. Soc.* **1973**, *95*, 5529−5539.

(4) Manriquez, J. M.; Fagan, P. J.; Marks, T. J. Bis-(Pentamethylcyclopentadienyl)Actinide Chemistry: Properties of Stable Thorium and Uranium Dialkyls and Hydrides. *J. Am. Chem. Soc.* **1978**, *100*, 3939−3941.

(5) Evans, W. J.; Kozimor, S. A.; Hillman, W. R.; Ziller, J. W. Synthesis and Structure of the Bis(Tetramethylcyclopentadienyl) Uranium Metallocenes $(C_5Me_4H)_2UMe_2$, $(C_5Me_4H)_2UMeCl$, $[(C_5Me_4H)_2U][(\mu\text{-}H_6\text{:}H_1\text{-}Ph)(\mu\text{-}H_1\text{:}H_1\text{-}Ph)BPh_2]$, and $[(C_5Me_4)\text{-}SiMe_2(CH_2CHCH_2)]_2UI(THF)$. *Organometallics* **2005**, *24*, 4676−4683.

(6) Jantunen, K. C.; Burns, C. J.; Castro-Rodriguez, I.; Da Re, R. E.; Golden, J. T.; Morris, D. E.; Scott, B. L.; Taw, F. L.; Kiplinger, J. L. Thorium(IV) and Uranium(IV) Ketimide Complexes Prepared by Nitrile Insertion into Actinide−Alkyl and − Aryl Bonds. *Organometallics* **2004**, *23*, 4682−4692.

(7) Stewart, J. L.; Andersen, R. A. Trivalent Uranium Chemistry: Molecular Structure of $[(Me_3Si)_2N]_3U$. *Polyhedron* **1998**, *17*, 953−958.

(8) Diaconescu, P. L.; Odom, A. L.; Agapie, T.; Cummins, C. C. Uranium−Group 14 Element Single Bonds: Isolation and Characterization of a Uranium(IV) Silyl Species. *Organometallics* **2001**, *20*, 4993−4995.

(9) Monreal, M. J.; Diaconescu, P. L. A Weak Interaction between Iron and Uranium in Uranium Alkyl Complexes Supported by Ferrocene Diamide Ligands. *Organometallics* **2008**, *27*, 1702−1706.

(10) Lewis, A. J.; Carroll, P. J.; Schelter, E. J. Stable Uranium(VI) Methyl and Acetylide Complexes and the Elucidation of an Inverse Trans Influence Ligand Series. *J. Am. Chem. Soc.* **2013**, *135*, 13185−13192.

(11) Stewart, J. L.; Andersen, R. A. Preparation and Crystal Structure of the Addition Compound $MeLi{\cdot}U[OCH(CMe_3)_2]_4$, a Compound with a Uranium to Carbon σ-Bond. *J. Chem. Soc., Chem. Commun.* **1987**, 1846−1847.

(12) Edwards, P. G.; Andersen, R. A.; Zalkin, A. Tertiary Phosphine Derivatives of the F-Block Metals. Preparation of $X_4M\text{-}(Me_2PCH_2CH_2PMe_2)_2$, Where X Is Halide, Methyl or Phenoxy and M Is Thorium or Uranium. Crystal Structure of Tetraphenoxybis-[Bis(1,2-Dimethylphosphino)Ethane]Uranium(IV). *J. Am. Chem. Soc.* **1981**, *103*, 7792−7794.

(13) Newell, B. S.; Schwaab, T. C.; Shores, M. P. Synthesis and Characterization of a Novel Tetranuclear 5f Compound: A New Synthon for Exploring U(IV) Chemistry. *Inorg. Chem.* **2011**, *50*, 12108−12115.

(14) Marks, T. J.; Seyam, A. M. Observations on the Thermal Decomposition of Some Uranium(IV) Tetraalkyls. *J. Organomet. Chem.* **1974**, *67*, 61−66.

(15) M. Seyam, A. Further Observations on the Reaction of Uranium Tetrachloride with Simple Lithium Alkyls. *Inorg. Chim. Acta* **1983**, *77*, L123−L125.

(16) Kraft, S. J.; Fanwick, P. E.; Bart, S. C. Carbon−Carbon Reductive Elimination from Homoleptic Uranium(IV) Alkyls Induced by Redox-Active Ligands. *J. Am. Chem. Soc.* **2012**, *134*, 6160−6168.

(17) Johnson, S. A.; Kiernicki, J. J.; Fanwick, P. E.; Bart, S. C. New Benzylpotassium Reagents and Their Utility for the Synthesis of Homoleptic Uranium(IV) Benzyl Derivatives. *Organometallics* **2015**, *34*, 2889−2895.

(18) Manriquez, J. M.; Fagan, P. J.; Marks, T. J.; Vollmer, S. H.; Day, C. S.; Day, V. W. Pentamethylcyclopentadienyl Organoactinides. Trivalent Uranium Organometallic Chemistry and the Unusual Structure of Bis(Pentamethylcyclopentadienyl)Uranium Monochloride. *J. Am. Chem. Soc.* **1979**, *101*, 5075−5078.

(19) Matson, E. M.; Forrest, W. P.; Fanwick, P. E.; Bart, S. C. Functionalization of Carbon Dioxide and Carbon Disulfide Using a Stable Uranium(III) Alkyl Complex. *J. Am. Chem. Soc.* **2011**, *133*, 4948−4954.

(20) Fortier, S.; Walensky, J. R.; Wu, G.; Hayton, T. W. High-Valent Uranium Alkyls: Evidence for the Formation of $U^{VI}(CH_2SiMe_3)_6$. *J. Am. Chem. Soc.* **2011**, *133*, 11732−11743.

(21) Fortier, S.; Kaltsoyannis, N.; Wu, G.; Hayton, T. W. Probing the Reactivity and Electronic Structure of a Uranium(V) Terminal Oxo Complex. *J. Am. Chem. Soc.* **2011**, *133*, 14224−14227.

(22) Bunker, B. C.; Drago, R. S.; Hendrickson, D. N.; Richman, R. M.; Kessell, S. L. Experimental Evidence for Trapped Valences in the Mixed-Valence Complex.Mu.-Pyrazine-Bis(Pentaammineruthenium) Tosylate. Electron Paramagnetic Resonance, Magnetic Susceptibility, and Nuclear Magnetic Resonance Results. *J. Am. Chem. Soc.* **1978**, *100*, 3805−3814.

(23) Boaretto, R.; Roussel, P.; Kingsley, A. J.; Munslow, I. J.; Sanders, C. J.; Alcock, N. W.; Scott, P. Structure and Reactions of a Metallacyclic Complex Containing a Remarkably Long Uranium−Carbon Bond. *Chem. Commun.* **1999**, 1701−1702.

DOI: 10.1021/acs.inorgchem.8b03175
Inorg. Chem. 2019, 58, 4152−4163

(24) Boaretto, R.; Roussel, P.; Alcock, N. W.; Kingsley, A. J.; Munslow, I. J.; Sanders, C. J.; Scott, P. Synthesis of a Highly Strained Uranacycle: Molecular Structures of Organometallic Products Arising from Reduction, Oxidation and Protonolysis. *J. Organomet. Chem.* **1999**, *591*, 174−184.
(25) Graves, C. R.; Scott, B. L.; Morris, D. E.; Kiplinger, J. L. Tetravalent and Pentavalent Uranium Acetylide Complexes Prepared by Oxidative Functionalization with CuC≡CPh. *Organometallics* **2008**, *27*, 3335−3337.
(26) Atwood, J. L.; Hains, C. F.; Tsutsui, M.; Gebala, A. E. X-Ray Crystallographic Characterization of the Uranium−Carbon σ-Bond in Tricyclopentadienylphenylethynyluranium(IV). *J. Chem. Soc., Chem. Commun.* **1973**, 452−453.
(27) Evans, W. J.; Walensky, J. R.; Ziller, J. W. Insertion Reactivity of CO_2, PhNCO, $Me_3CC{\equiv}N$, and $Me_3CN{\equiv}C$ with the Uranium−Alkynyl Bonds in $(C_5Me_5)_2U(C{\equiv}CPh)_2$. *Organometallics* **2010**, *29*, 945−950.
(28) Atwood, J. L.; Tsutsui, M.; Ely, N.; Gebala, A. E. The Crystal and Molecular Structure of Tricyclopentadienylethynyluranium(IV). *J. Coord. Chem.* **1976**, *5*, 209−215.
(29) Montalvo, E.; Ziller, J. W.; DiPasquale, A. G.; Rheingold, A. L.; Evans, W. J. Utility of the 1,3,4,6,7,8-Hexahydro-2H-Pyrimido[1,2-a]Pyrimidinato Ligand, $(Hpp)^-$, in Stabilizing Uranium Metallocene Mono-Alkyl and "Tuck-in" Complexes. *Organometallics* **2010**, *29*, 2104−2110.
(30) Evans, W. J.; Walensky, J. R.; Ziller, J. W.; Rheingold, A. L. Insertion of Carbodiimides and Organic Azides into Actinide−Carbon Bonds. *Organometallics* **2009**, *28*, 3350−3357.
(31) Evans, W. J.; Siladke, N. A.; Ziller, J. W. Reactivity of the Tethered Alkyl Uranium Bonds of $(\eta^5{:}\kappa^1\text{-}C_5Me_4SiMe_2CH_2)_2U$. *C. R. Chim.* **2010**, *13*, 775−780.
(32) Thomson, R. K.; Graves, C. R.; Scott, B. L.; Kiplinger, J. L. Noble Reactions for the Actinides: Safe Gold-Based Access to Organouranium and Azido Complexes. *Eur. J. Inorg. Chem.* **2009**, 1451−1455.
(33) Matson, E. M.; Fanwick, P. E.; Bart, S. C. Formation of Trivalent U−C, U−N, and U−S Bonds and Their Reactivity toward Carbon Dioxide and Acetone. *Organometallics* **2011**, *30*, 5753−5762.
(34) Seaman, L. A.; Hrobárik, P.; Schettini, M. F.; Fortier, S.; Kaupp, M.; Hayton, T. W. A Rare Uranyl(VI)−Alkyl Ate Complex $[Li(DME)_{1.5}]_2[UO_2(CH_2SiMe_3)_4]$ and Its Comparison with a Homoleptic Uranium(VI)−Hexaalkyl. *Angew. Chem., Int. Ed.* **2013**, *52*, 3259−3263.
(35) Cooper, O. J.; Mills, D. P.; McMaster, J.; Tuna, F.; McInnes, E. J. L.; Lewis, W.; Blake, A. J.; Liddle, S. T. The Nature of the U = C Double Bond: Pushing the Stability of High-Oxidation-State Uranium Carbenes to the Limit. *Chem. - Eur. J.* **2013**, *19*, 7071−7083.
(36) Hrobárik, P.; Hrobáriková, V.; Greif, A. H.; Kaupp, M. Giant Spin-Orbit Effects on NMR Shifts in Diamagnetic Actinide Complexes: Guiding the Search of Uranium(VI) Hydride Complexes in the Correct Spectral Range. *Angew. Chem., Int. Ed.* **2012**, *51*, 10884−10888.
(37) Greif, A. H.; Hrobárik, P.; Autschbach, J.; Kaupp, M. Giant Spin−Orbit Effects on ^1H and ^{13}C NMR Shifts for Uranium(VI) Complexes Revisited: Role of the Exchange−Correlation Response Kernel, Bonding Analyses, and New Predictions. *Phys. Chem. Chem. Phys.* **2016**, *18*, 30462−30474.
(38) Smiles, D. E.; Wu, G.; Hrobárik, P.; Hayton, T. W. Use of ^{77}Se and ^{125}Te NMR Spectroscopy to Probe Covalency of the Actinide-Chalcogen Bonding in $[Th(E_n)\{N(SiMe_3)_2\}_3]^-$ (E = Se, Te; n = 1, 2) and Their Oxo-Uranium(VI) Congeners. *J. Am. Chem. Soc.* **2016**, *138*, 814−825.
(39) Arnold, P. L.; Farnaby, J. H.; White, R. C.; Kaltsoyannis, N.; Gardiner, M. G.; Love, J. B. Switchable π-Coordination and C−H Metallation in Small-Cavity Macrocyclic Uranium and Thorium Complexes. *Chem. Sci.* **2014**, *5*, 756−765.
(40) Arnold, P. L.; Prescimone, A.; Farnaby, J. H.; Mansell, S. M.; Parsons, S.; Kaltsoyannis, N. Characterizing Pressure-Induced Uranium C-H Agostic Bonds. *Angew. Chem., Int. Ed.* **2015**, *54*, 6735−6739.
(41) Arnold, P. L.; Turner, Z. R.; Kaltsoyannis, N.; Pelekanaki, P.; Bellabarba, R. M.; Tooze, R. P. Covalency in Ce^{IV} and U^{IV} Halide and N-Heterocyclic Carbene Bonds. *Chem. - Eur. J.* **2010**, *16*, 9623−9629.
(42) Brown, J. L.; Fortier, S.; Wu, G.; Kaltsoyannis, N.; Hayton, T. W. Synthesis and Spectroscopic and Computational Characterization of the Chalcogenido-Substituted Analogues of the Uranyl Ion, $[OUE]^{2+}$ (E = S, Se). *J. Am. Chem. Soc.* **2013**, *135*, 5352−5355.
(43) Kirker, I.; Kaltsoyannis, N. Does Covalency Really Increase across the 5f Series? A Comparison of Molecular Orbital, Natural Population, Spin and Electron Density Analyses of $AnCp_3$ (An = Th−Cm; Cp = $H_5\text{-}C_5H_5$). *Dalton Trans.* **2011**, *40*, 124−131.
(44) Mountain, A. R. E.; Kaltsoyannis, N. Do QTAIM Metrics Correlate with the Strength of Heavy Element−Ligand Bonds? *Dalton Trans.* **2013**, *42*, 13477−13486.
(45) Jones, M. B.; Gaunt, A. J.; Gordon, J. C.; Kaltsoyannis, N.; Neu, M. P.; Scott, B. L. Uncovering f-Element Bonding Differences and Electronic Structure in a Series of 1:3 and 1:4 Complexes with a Diselenophosphinate Ligand. *Chem. Sci.* **2013**, *4*, 1189−1203.
(46) Smiles, D. E.; Wu, G.; Hrobárik, P.; Hayton, T. W. Synthesis, Thermochemistry, Bonding, and ^{13}C NMR Chemical Shift Analysis of a Phosphorano-Stabilized Carbene of Thorium. *Organometallics* **2017**, *36*, 4519−4524.
(47) Drago, R. S.; Zink, J. I.; Richman, R. M.; Perry, W. D. Theory of Isotropic Shifts in the Nmr of Paramagnetic Materials: Part I. *J. Chem. Educ.* **1974**, *51*, 371.
(48) Le Guennic, B.; Floyd, T.; Galan, B. R.; Autschbach, J.; Keister, J. B. Paramagnetic Effects on the NMR Spectra of "Diamagnetic" Ruthenium(Bis-Phosphine)(Bis-Semiquinone) Complexes. *Inorg. Chem.* **2009**, *48*, 5504−5511.
(49) Hansch, C.; Leo, A.; Taft, R. W. A Survey of Hammett Substituent Constants and Resonance and Field Parameters. *Chem. Rev.* **1991**, *91*, 165−195.
(50) Kaupp, M.; Malkina, O. L.; Malkin, V. G.; Pyykkö, P. How Do Spin−Orbit-Induced Heavy-Atom Effects on NMR Chemical Shifts Function? Validation of a Simple Analogy to Spin−Spin Coupling by Density Functional Theory (DFT) Calculations on Some Iodo Compounds. *Chem. - Eur. J.* **1998**, *4*, 118−126.
(51) Hrobárik, P.; Hrobáriková, V.; Meier, F.; Repiský, M.; Komorovský, S.; Kaupp, M. Relativistic Four-Component DFT Calculations of ^1H NMR Chemical Shifts in Transition-Metal Hydride Complexes: Unusual High-Field Shifts Beyond the Buckingham−Stephens Model. *J. Phys. Chem. A* **2011**, *115*, 5654−5659.
(52) Greif, A. H.; Hrobárik, P.; Hrobáriková, V.; Arbuznikov, A. V.; Autschbach, J.; Kaupp, M. A Relativistic Quantum-Chemical Analysis of the Trans Influence on ^1H NMR Hydride Shifts in Square-Planar Platinum(II) Complexes. *Inorg. Chem.* **2015**, *54*, 7199−7208.
(53) Pedrick, E. A.; Hrobárik, P.; Seaman, L. A.; Wu, G.; Hayton, T. W. Synthesis, Structure and Bonding of Hexaphenyl Thorium(IV): Observation of a Non-Octahedral Structure. *Chem. Commun.* **2016**, *52*, 689−692.
(54) Greif, A. H.; Hrobárik, P.; Kaupp, M. Insights into Trans-Ligand and Spin-Orbit Effects on Electronic Structure and Ligand NMR Shifts in Transition-Metal Complexes. *Chem. - Eur. J.* **2017**, *23*, 9790−9803.
(55) Rocchigiani, L.; Fernandez-Cestau, J.; Chambrier, I.; Hrobárik, P.; Bochmann, M. Unlocking Structural Diversity in Gold(III) Hydrides: Unexpected Interplay of Cis/Trans-Influence on Stability, Insertion Chemistry, and NMR Chemical Shifts. *J. Am. Chem. Soc.* **2018**, *140*, 8287−8302.
(56) Vícha, J.; Komorovský, S.; Repiský, M.; Marek, R.; Straka, M. Relativistic Spin−Orbit Heavy Atom on the Light Atom NMR Chemical Shifts: General Trends Across the Periodic Table Explained. *J. Chem. Theory Comput.* **2018**, *14*, 3025−3039.
(57) In this particular case, the small upfield shifts calculated upon artificial U−C bond shortening, while keeping R unchanged, can be explained by a minor charge accumulation at the U−C acetylide

DOI: 10.1021/acs.inorgchem.8b03175
Inorg. Chem. 2019, 58, 4152−4163

carbon as well as by an increase of the energy gaps between magnetically coupled metal−ligand bonding MOs and vacant orbitals (see q(C) and ΔE values in Table S8 in the Supporting Information as a function of U−C bond distance). Note that this effect is somewhat more pronounced for the σ^{SO} contribution, which is inversely proportional to the square of the energy separation between the magnetically coupled orbitals ($1/\Delta E^2$). Nevertheless, the variation of ΔE for minima of structurally related series remains sufficiently constant, which allows correlation of chemical shifts with local properties, such as atomic charges or bond covalencies.

(58) Ramsey, N. F. Magnetic Shielding of Nuclei in Molecules. *Phys. Rev.* **1950**, *78*, 699−703.

(59) Karplus, M.; Pople, J. A. Theory of Carbon NMR Chemical Shifts in Conjugated Molecules. *J. Chem. Phys.* **1963**, *38*, 2803−2807.

(60) Atkins, P. W.; Friedman, R. S. *Molecular Quantum Mechanics*, 3rd ed.; Oxford University Press: Oxford, UK, 1997.

(61) Hutchison, C. A.; Tsang, T.; Weinstock, B. Magnetic Susceptibility of Neptunium Hexafluoride in Uranium Hexafluoride. *J. Chem. Phys.* **1962**, *37*, 555−562.

(62) McGlynn, S. P.; Smith, J. K. The Electronic Structure, Spectra, and Magnetic Properties of Actinyl Ions. *J. Mol. Spectrosc.* **1961**, *6*, 164−187.

(63) Burrows, H. D.; Kemp, T. J. The Photochemistry of the Uranyl Ion. *Chem. Soc. Rev.* **1974**, *3*, 139−165.

(64) Carrington, A. The Temperature-Independent Paramagnetism of Permanganate and Related Complexes. *Mol. Phys.* **1960**, *3*, 271−275.

(65) Fowler, P. W.; Steiner, E. Temperature-Independent Paramagnetism in Closed-Shell Oxanions of First-Row Transition Metals. *J. Chem. Soc., Faraday Trans.* **1993**, *89*, 1915−1924.

(66) Figgis, B. N.; Kidd, R. G.; Nyholm, R. S. Oxygen-17 Nuclear Magnetic Resonance of Inorganic Compounds. *Proc. R. Soc. London., Ser. A* **1962**, *269*, 469−480.

(67) Kaupp, M.; Malkin, V. G.; Malkina, O. L.; Salahub, D. R. Scalar Relativistic Effects on ^{17}O NMR Chemical Shifts in Transition-Metal Oxo Complexes. An Ab Initio ECP/DFT Study. *J. Am. Chem. Soc.* **1995**, *117*, 1851−1852.

(68) Kaupp, M.; Malkina, O. L.; Malkin, V. G. The Calculation of ^{17}O Chemical Shielding in Transition Metal Oxo Complexes. I. Comparison of DFT and Ab Initio Approaches, and Mechanisms of Relativity-Induced Shielding. *J. Chem. Phys.* **1997**, *106*, 9201−9212.

(69) Graves, C. R.; Vaughn, A. E.; Schelter, E. J.; Scott, B. L.; Thompson, J. D.; Morris, D. E.; Kiplinger, J. L. Probing the Chemistry, Electronic Structure and Redox Energetics in Organometallic Pentavalent Uranium Complexes. *Inorg. Chem.* **2008**, *47*, 11879−11891.

(70) Graves, C. R.; Yang, P.; Kozimor, S. A.; Vaughn, A. E.; Clark, D. L.; Conradson, S. D.; Schelter, E. J.; Scott, B. L.; Thompson, J. D.; Hay, P. J.; Morris, D. E.; Kiplinger, J. L. Organometallic Uranium(V)−Imido Halide Complexes: From Synthesis to Electronic Structure and Bonding. *J. Am. Chem. Soc.* **2008**, *130*, 5272−5285.

(71) Matson, E. M.; Forrest, W. P.; Fanwick, P. E.; Bart, S. C. Use of Alkylsodium Reagents for the Synthesis of Trivalent Uranium Alkyl Complexes. *Organometallics* **2012**, *31*, 4467−4473.

(72) Avens, L. R.; Bott, S. G.; Clark, D. L.; Sattelberger, A. P.; Watkin, J. G.; Zwick, B. D. A Convenient Entry into Trivalent Actinide Chemistry: Synthesis and Characterization of $AnI_3(THF)_4$ and $An[N(SiMe_3)_2]_3$ (An = U, Np, Pu). *Inorg. Chem.* **1994**, *33*, 2248−2256.

(73) Theunissen, C.; Lecomte, M.; Jouvin, K.; Laouiti, A.; Guissart, C.; Heimburger, J.; Loire, E.; Evano, G. Convenient and Practical Alkynylation of Heteronucleophiles with Copper Acetylides. *Synthesis* **2014**, *46*, 1157−1166.

(74) *SAINT*; Bruker AXS Inc: Madison, WI, 2009.

(75) *SHELXTL*; Bruker AXS Inc.: Madison, WI, 2009.

(76) Sheldrick, G. M. *TWINABS*; University of Gottingen: Gottingen, Germany, 2008.

(77) Sheldrich, G. M. *SADABS*; University of Gottingen: Gottingen, Germany, 2007.

(78) Sheldrick, G. M. A Short History of *SHELX*. *Acta Crystallogr., Sect. A: Found. Crystallogr.* **2008**, *64*, 112−122.

(79) Becke, A. D. Density-functional Thermochemistry. III. The Role of Exact Exchange. *J. Chem. Phys.* **1993**, *98*, 5648−5652.

(80) Lee, C.; Yang, W.; Parr, R. G. Development of the Colle-Salvetti Correlation-Energy Formula into a Functional of the Electron Density. *Phys. Rev. B: Condens. Matter Mater. Phys.* **1988**, *37*, 785−789.

(81) Stephens, P. J.; Devlin, F. J.; Chabalowski, C. F.; Frisch, M. J. Ab Initio Calculation of Vibrational Absorption and Circular Dichroism Spectra Using Density Functional Force Fields. *J. Phys. Chem.* **1994**, *98*, 11623−11627.

(82) Grimme, S.; Antony, J.; Ehrlich, S.; Krieg, H. A Consistent and Accurate Ab Initio Parametrization of Density Functional Dispersion Correction (DFT-D) for the 94 Elements H-Pu. *J. Chem. Phys.* **2010**, *132*, 154104.

(83) Grimme, S.; Ehrlich, S.; Goerigk, L. Effect of the Damping Function in Dispersion Corrected Density Functional Theory. *J. Comput. Chem.* **2011**, *32*, 1456−1465.

(84) *TURBOMOLE*, version 7.0.2; University of Karlsruhe and Forschungszentrum Karlsruhe GmbH, 1989−2007; TURBOMOLE GmbH, since 2007. Available from http://www.turbomole.com.

(85) Cao, X.; Dolg, M. Segmented Contraction Scheme for Small-Core Actinide Pseudopotential Basis Sets. *J. Mol. Struct.: THEOCHEM* **2004**, *673*, 203−209.

(86) Weigend, F.; Ahlrichs, R. Balanced Basis Sets of Split Valence, Triple Zeta Valence and Quadruple Zeta Valence Quality for H to Rn: Design and Assessment of Accuracy. *Phys. Chem. Chem. Phys.* **2005**, *7*, 3297−3305.

(87) *Amsterdam Density Functional (ADF)*, version 2017.112, SCM; Theoretical Chemistry, Vrije Universiteit: Amsterdam, Netherlands, 2018. Available from http://www.scm.com.

(88) Perdew, J. P.; Burke, K.; Ernzerhof, M. Generalized Gradient Approximation Made Simple. *Phys. Rev. Lett.* **1996**, *77*, 3865−3868.

(89) Perdew, J. P.; Burke, K.; Ernzerhof, M. Generalized Gradient Approximation Made Simple [Phys. Rev. Lett. 77, 3865 (1996)]. *Phys. Rev. Lett.* **1997**, *78*, 1396−1396.

(90) Adamo, C.; Barone, V. Toward Chemical Accuracy in the Computation of NMR Shieldings: The PBE0 Model. *Chem. Phys. Lett.* **1998**, *298*, 113−119.

(91) Schreckenbach, G.; Ziegler, T. Calculation of NMR Shielding Tensors Using Gauge-Including Atomic Orbitals and Modern Density Functional Theory. *J. Phys. Chem.* **1995**, *99*, 606−611.

(92) Wolff, S. K.; Ziegler, T. Calculation of DFT-GIAO NMR Shifts with the Inclusion of Spin-Orbit Coupling. *J. Chem. Phys.* **1998**, *109*, 895−905.

(93) Wolff, S. K.; Ziegler, T.; van Lenthe, E.; Baerends, E. J. Density Functional Calculations of Nuclear Magnetic Shieldings Using the Zeroth-Order Regular Approximation (ZORA) for Relativistic Effects: ZORA Nuclear Magnetic Resonance. *J. Chem. Phys.* **1999**, *110*, 7689−7698.

(94) Krykunov, M.; Ziegler, T.; van Lenthe, E. Hybrid Density Functional Calculations of Nuclear Magnetic Shieldings Using Slater-Type Orbitals and the Zeroth-Order Regular Approximation. *Int. J. Quantum Chem.* **2009**, *109*, 1676−1683.

(95) Hansen, A. E.; Bouman, T. D. Localized Orbital/Local Origin Method for Calculation and Analysis of NMR Shieldings. Applications to ^{13}C Shielding Tensors. *J. Chem. Phys.* **1985**, *82*, 5035−5047.

(96) Reed, A. E.; Curtiss, L. A.; Weinhold, F. Intermolecular Interactions from a Natural Bond Orbital, Donor-Acceptor Viewpoint. *Chem. Rev.* **1988**, *88*, 899−926.

(97) Glendening, E. D.; Badenhoop, J. K.; Reed, A. E.; Carpenter, J. E.; Bohmann, J. A.; Morales, C. M.; Landis, C. R.; Weinhold, F. *NBO 6.0*; Theoretical Chemistry Institute, University of Wisconsin: Madison, WI, 2013. Available from http://nbo6.chem.wisc.edu/.

(98) Frisch, M. J.; Trucks, G. W.; Schlegel, H. B.; Scuseria, G. E.; Robb, M. A.; Cheeseman, J. R.; Scalmani, G.; Barone, V.; Mennucci, B.; Petersson, G. A.; Nakatsuji, H.; Caricato, M.; Li, X.; Hratchian, H. P.; Izmaylov, A. F.; Bloino, J.; Zheng, G.; Sonnenberg, J. L.; Hada, M.;

DOI: 10.1021/acs.inorgchem.8b03175
Inorg. Chem. 2019, 58, 4152−4163

Ehara, M.; Toyota, K.; Fukuda, R.; Hasegawa, J.; Ishida, M.; Nakajima, T.; Honda, Y.; Kitao, O.; Nakai, H.; Vreven, T.; Montgomery, J. A., Jr.; Peralta, J. E.; Ogliaro, F.; Bearpark, M.; Heyd, J. J.; Brothers, E.; Kudin, K. N.; Staroverov, V. N.; Kobayashi, R.; Normand, J.; Raghavachari, K.; Rendell, A.; Burant, J. C.; Iyengar, S. S.; Tomasi, J.; Cossi, M.; Rega, N.; Millam, N. J.; Klene, M.; Knox, J. E.; Cross, J. B.; Bakken, V.; Adamo, C.; Jaramillo, J.; Gomperts, R.; Stratmann, R. E.; Yazyev, O.; Austin, A. J.; Cammi, R.; Pomelli, C.; Ochterski, J. W.; Martin, R. L.; Morokuma, K.; Zakrzewski, V. G.; Voth, G. A.; Salvador, P.; Dannenberg, J. J.; Dapprich, S.; Daniels, A. D.; Farkas, Ö.; Foresman, J. B.; Ortiz, J. V.; Cioslowski, J.; Fox, D. J. *Gaussian 09*, revision D.01; Gaussian, Inc.: Wallingford, CT, 2009.

(99) Bader, R. F. W.; Stephens, M. E. Spatial Localization of the Electronic Pair and Number Distributions in Molecules. *J. Am. Chem. Soc.* **1975**, *97*, 7391−7399.

(100) Bader, R. F. W. *Atoms in Molecules: A Quantum Theory*; Oxford University Press: Oxford, UK, 1990.

(101) Matta, C. F.; Boyd, R. J. *The Quantum Theory of Atoms and Molecules*; Wiley-VCH: Weinheim, Germany, 2007.

(102) (a) Lu, T. *Multiwfn: A Multifunctional Wave Function Analyzer*, version 3.5; Beijing Kein Research Center for Natural Sciences, 2018. Available from http://sobereva.com/multiwfn. (b) Lu, T.; Chen, F. W. J. *J. Comput. Chem.* **2012**, *33*, 580−592.

DOI: 10.1021/acs.inorgchem.8b03175
Inorg. Chem. 2019, 58, 4152−4163